Shi, Shuyu; Sigg, Stephan; Chen, Lin; Ji, Yusheng

Accurate Location Tracking from CSI-based Passive Device-free Probabilistic Fingerprinting

Accurate Location Tracking from CSI-based Passive Device-free Probabilistic Fingerprinting

Shuyu Shi[1,5], Stephan Sigg[2], Lin Chen[3,4] and Yusheng Ji[1]

[1]National Institute of Informatics, Tokyo, Japan

[2]Aalto University, Aalto, Finland

[3]Department of Electrical Engineering, Yale University, New Haven, CT, USA

[4]Institute of Network Computing and Information System, School of EECS, Peking University, Beijing, China

[5]School of Computer Science and Engineering, Nanyang Technological University (NTU), Singapore

Abstract—The research on indoor localization has received great interest in recent years. This has been fuelled by the ubiquitous distribution of electronic devices equipped with a radio frequency (RF) interface. Analyzing the signal fluctuation on the RF-interface can, for instance, solve the still open issue of ubiquitous reliable indoor localization and tracking. Device bound and device free approaches with remarkable accuracy have been reported recently.

In this paper, we present an accurate device-free passive (DfP) indoor location tracking system which adopts channel state information (CSI) readings from off-the-shelf WiFi 802.11n wireless cards. The fine-grained subchannel measurements for MIMO-OFDM PHY layer parameters are exploited to improve localization and tracking accuracy. To enable precise positioning in the presence of heavy multipath effects in cluttered indoor scenarios, we experimentally validate the unpredictability of CSI measurements and suggest a probabilistic fingerprint-based technique as an accurate solution. Our scheme further boosts the localization efficiency by using principal component analysis (PCA) to filter the most relevant feature vectors. Furthermore, with Bayesian filtering, we continuously track the trajectory of a moving subject. We have evaluated the performance of our system in four indoor environments and compared it with state-of-art indoor localization schemes. Our experimental results demonstrate that this complex channel information enables more accurate localization of non-equipped individuals.

I. Introduction

People assign a significant share of their time indoors (over 80%) [1], covering shopping in leisure time or attending meetings during office hours. Accurate information on mobility patterns and movement paths would enable improved building and path management and also help to advertise relevant information at right places. However, in most practical purposes, it can not be assumed that all subjects to be tracked can be equipped in advance, as this would require considerable resources. Recent research on RF-based indoor localization, however, has let to promising results. In these approaches, fluctuations in the ubiquitously available RF-Signals are exploited for localization and tracking purposes.

Traditional approaches require transceiver-equipped subjects and localize the device rather than its wearer by translating the observed changes and fluctuation in received signals to a coordinate system.

Examples are FM-based indoor localization [8], GSM-based techniques [26] as well as Bluetooth [13] or WiFi-based

systems [4]. The reported localization accuracy of state-of-art device-bound indoor systems is less than $0.5m$ [32] [33] with the adoption of CSI information, which meets the demand of most applications.

The main disadvantage of such approaches is, however, that all require a cooperating and equipped subject to be localized. However, in most practical purposes, it can not be assumed that all subjects to be tracked can be equipped in advance, since this would require considerable resources. A possible alternative is device-free passive (DfP) indoor localization [52], [7], [49], [31]. In DfP indoor localization, fingerprint-based techniques are widely adopted, since the unpredictability of radio propagation due to multipath effects renders the alternative of analyzing RF signals challenging. Among these solutions, the *Nuzzer* system [31] builds an offline radio map by modeling the RSSI of a data stream from an AP-MP pair to follow Gaussian distribution and assuming all the data streams to be independent at each predefined training location. In the online phase, a location is determined whose RSS samples match closely with the passive radio map. *PC-DfP* improves the accuracy by adopting linear discriminant analysis or quadratic discriminant analysis. Channel state information (CSI) recently can be aggregated from a commodity Intel 5300 Network Interface Card in the granularity of OFDM subchannels, a much finer grained channel indicator than RSSI. By adopting the raw CSI measurements, a recent work, *Pilot*, shows that the *correlation* feature of CSI samples can be leveraged to distinguish between empty environment and presence of a subject in the area of interest, and further determine the location of this subject. Thanks to the fine-resolution of CSI readings, *Pilot* outperforms state-of-art RSSI-based indoor schemes, such as *Nuzzer* and *PC-DfP*. However, for one CSI reading from a packet, only one correlation value is calculated in *Pilot*, which does not take full advantage of the characteristics in frequency and space domain.

In this study, we further advance CSI-based indoor localization by adopting every single subchannel amplitude of CSI measurements and propose a single-stage direct classification. This is in contrast to *Pilot*, which utilizes the "*correlation*" between multiple CSI readings in a two-stage process. The contributions of this paper are

  a) a comprehensive analysis of the characteristics of CSI

change induced by human presence.

b) a computationally efficient single-stage approach for indoor localization and tracking which takes full advantage of information provided by CSI measurements from commodity 802.11n WiFi wireless cards. The approach is computationally efficient and robust against high-dimensional CSI vectors due to PCA-based dimensionality reduction.

c) a large case study covering four diverse typical indoor spaces in two different buildings

d) a performance comparison to the state-of-art indoor positioning solutions *Nuzzer* [31], *PC-DfP* [50] and *Pilot* [46].

e) Kalman-filter and Particle-filter based approaches to track a moving target and a discussion on the adaptability of these two Bayesian filters to distinct walking patterns.

f) the Cramér-Rao Bound (CRB) on the proposed tracking system, which is regarded as the benchmark for asserting the performance of KF and PF based tracking algorithms.

This paper is an extension of our work presented in [34]. In particular, we have significantly revised and improved the analysis, conducted a more general experimental study in 4 diverse environments, added performance metrics for the analysis, compared the results achieved to two additional state-of-the-art algorithms, namely Nuzzer and PC-DfP and improved the overall discussion on the topic. Finally, and most significantly, our current system is able to continuously track a moving target. This is possible by the adaptation of Kalman-filter and Particle-Filter-based approaches. Both have been concisely investigated and are discussed in depth in this article.

The rest of this paper is structured as follows. The related work and preliminary studies are detailed in section II and III. In section IV, we describe the implementation of our proposed CSI-based passive device-free indoor localization system. In section V, we investigate the feasibility of tracking a moving person using Bayesian filtering. We detail the experiment setup in section VI. The evaluation results are presented in section VII. In Section VIII, related issues and possible solutions are discussed. Finally, section IX draws our conclusion and discusses future work.

II. RELATED WORK

Recently, location estimation in indoor environments has gained a great deal of attention by researchers, due to the increasing demand of location-based services and applications. While a large range of information sources have been utilized, such as video [20], magnetometers [22], and magnetic resonant coupling [27], all of which suffer from the system cost and installation effort. In this study, of particular interest are radio frequency (RF) based solutions, as RF-channel information is a ubiquitously available source, thereby mitigating installation cost. Many systems using RF signals have been designed for precise indoor positioning from traditional device-bound solutions. In these, the target is an RF-transceiver equipped subject [31], [50], [25], [46]. We detail these two categories of localization systems in the following. Furthermore, we survey a plethora of methods for tracking the trajectory of a moving person using RF sources.

A. Device-bound Localization

Device-bound localization systems deal with the problem of positioning an entity equipped with an RF-emitting device. Researchers working in this direction propose to use different wireless techniques ranging from Infrared (IR) [40], Ultrasonic [18], RFID [24], Bluetooth [13] or WiFi [4], [44], [6], [48]. Among these, WiFi signals are most widely adopted due to popularity and low cost. For example, as described in [4], the proposed RADAR system first builds an a priori fingerprint map by gathering the WiFi RSS measurements at different locations in the training phase, and then deduces the location by minimizing the Euclidean distance between online RSS measurements and corresponding measurements in the radio map during the test phase. The accuracy can be further improved by using CSI measurements from revised commodity WiFi devices and clustering techniques for localization [32] [33], where experimental evaluation asserts error distances smaller than $0.5m$. Recently, Xie et al. [47] and Vasisht et al. [38] released new tools, *Splicer* and *Chronos* respectively, both of which can measure the CSIs from a much wider spectrum band and adjust the errors of amplitude and phase of the gathered CSIs, further improving the precision of indoor localization. Except for the utilization of fine-grained CSI measurements, in order to improve the positioning accuracy, some recent studies propose to either exploit other extra wireless signal measurements [47] or to design a novel scheme for accurate fingerprint generation [44]. Apart from accuracy, efficiency of location estimation is of significant importance for a positioning system as well. To this end, Cai et al. [6] introduce CRIL, which can quickly adapt to the changes of dynamic environments and thus improve the efficiency of an indoor localization system while preserving the localization accuracy.

B. Device-free Localization

The assumption that a device is always carried by a subject is not realistic. A device-free system was first introduced by Youssef et. al [51] for the localization of a non-equipped entity. In recent years, various RF device-free localization schemes have been proposed [51], [49], [46], [42], [43], [19]. These schemes mainly constitute *fingerprint-based* and *model-based* solutions. Model-based algorithms use statistical models to establish a mathematical relationship between the radio signals and the location in indoor environments and thus do not require the laborious effort to construct and maintain the radio map. However, in most cases, due to the cluttered indoor environments, an accurate model cannot be built to capture the complicated relationship between radio signals and coordinates of indoor spaces. On the other hand, fingerprint-based algorithms do not assume any prior knowledge of the relationship between RF signals and positions while requiring considerable effort to construct and calibrate the radio map. We focus on the most relevant systems below.

Fingerprint-based indoor localization systems require to construct an offline radio map, and then compare it with the

collected online measurements to estimate the location of the targeted person [51], [49], [46], [31]. Seifeldin et. al [31] present an RSS-based large-scale device-free localization system, *Nuzzer,* by analyzing the human-induced RSS statistics with probabilistic techniques. It presumes the RSSI samples of each AP-MP stream to be Gaussian distribution. Furthermore, Xu et. al [49] employ linear discriminant analysis from RSS to recognize different cells of locations, which significantly mitigates NLoS effects and thereby achieves better accuracy in cluttered indoor environments. Furthermore, to ease the effort of building a radio map, a transferring positioning model based device-free system is proposed in [25], which can collect training measurements in a certain indoor environment and apply them into other different indoor spaces with the aid of floor plans. Also, some other studies try to construct radio maps using simultaneous localization and mapping (SLAM) approaches [14], [17]. In order to better characterize the influence of the target on wireless signals and extract suitable statistical features, Wang et. al [39] propose a deep learning approach to automatically learn discriminative features. With the evolution of WiFi PHY layer techniques, Xiao et al. [46] initially estimate the position of a passive entity from CSI-related patterns. On observing that CSI samples are susceptible to presence of a subject and immune to temporal variance, the authors propose the *Pilot* system to utilize correlations of CSI from 802.11n wireless cards as the discriminant feature to determine the location of passive subjects by a two-stage detection approach. Since CSI measurements provide more accurate channel information, the reported localization precision is dramatically increased compared to that achieved by other state-of-art RSS-based schemes. While the correlation feature enables the classification among different locations, it only represents the temporal characteristics of motion-induced variance of CSI samples. Furthermore, in *Pilot*, an abnormal environment should be detected by determining whether the correlation between the current CSI sample and normal CSI readings is smaller than a manually selected threshold before triggering the second-stage localization process. In this work, we propose a probabilistic fingerprint-based DfP localization scheme to analyze human-induced variance of CSI measurements. Differing from *Pilot,* we model the CSI change vector as a multivariate Gaussian distribution. Our system is further capable of tracking the trajectory of an individual by the adoption of Bayesian filtering techniques.

In terms of model-based localization systems, an approximate model is required upon which the localization algorithms can map the changes of RF measurements to the location of a targeted person [42], [43], [19]. For instance, Wilson and Patwari utilize Radio Tomographic Imaging (RTI) on the two-way RSS variance [42] or RSS mean fluctuations [43] between nodes arranged in a rectangle surrounding the monitored area for robust localization. To reduce the density of RF nodes, they develop a novel solution using RF transceivers in motion [19]. Recently, Kaltiokallio et. al [21] propose to model the RSS measurements of the indoor radio propagation channel as a three-state process, which can further increase the localization accuracy. Instead of leveraging RSSI measurements as raw source, Qian et. al [28] introduce a novel system Widar, which,

by modeling the relationship between the CSI measurements and the user's location and velocity, can yield a decimeter-level accuracy.

C. Device-free Tracking

Regarding mobility tracking systems, a generic approach is to exploit the multiple measurements in time series to reduce the positioning errors iteratively [12], [9]. In terms of device-free tracking systems, several solutions have been proposed [42], [53], [5]. For instance, in [42], [53], the authors exploit the Kalman filter for tracking a single person using the location results from Variance-based RTI and subspace Variance-based radio tomography respectively. Furthermore, they extend their work to track multiple persons [5]. Instead of using Kalman filter, the problem of tracking multiple persons is formulated as a data assignment problem (DAP) and solved by minimizing the total cost of DAP.

III. BACKGROUND AND MOTIVATION

A. Channel State Information

In the standard of the 802.11 protocol, RSS is defined as an indicator for the quality of a link, which characterizes the overall received signal power in the channel. With the wide adoption of multiple input multiple output-orthogonal frequency-division multiplexing (MIMO-OFDM) PHY technology in many wifi-class devices, RSS is no longer regarded as an accurate metric, since the data streams are transmitted on various orthogonal subchannels independently and the quality of these subchannels differs one by one. In contrast to RSS, CSI contains link information in the granularity of a single MIMO-OFDM subcarrier. Therefore, it holds the potential for more accurate indoor localization. With the release of the CSI tool for commodity WiFi cards by Halperin et. al [16], we can aggregate both the amplitude and phase information for each MIMO-OFDM subcarrier. Let t, r be the number of transmit (TX) and receive (RX) antennas, and w the total number of subcarriers for a TX-RX pair. Based on the functionality of the CSI tool, a CSI vector can be obtained per packet, containing $t \cdot r \cdot w$ values of subchannels as $\mathcal{C} = \{\mathcal{C}_{i,k}^m\}$, $i \in [1, t]$, $k \in [1, r]$, $m \in [1, w]$, for each value $\mathcal{C}_{i,k}^m$, it reflects both amplitude and phase of the RF signal $\mathcal{C}_{i,k}^m = |\mathcal{C}_{i,k}^m|e^{j \sin \theta}$ modulated at the subchannel m from transmit antenna i to receive antenna k.

The received signal strength (RSS) is a practical metric for the quality of a link, which characterizes the overall received signal power in the channel. As shown in Figure 1, RSS estimation can be acquired from the overall received channel power (e.g 8-bit information in WiFi 802.11 standards). With the adoption of OFDM modulation, as depicted in Figure 1, the CSI estimation can be obtained from reference signals (RSs) transmitted over various subcarriers. Thus, in contrast with RSS, it can represent the link quality in the granularity of subcarriers independently.

B. Unpredictable Nature of CSI in Indoor Environments

It is of great importance to know the sources of errors and biases to design a robust indoor localization system. Regarding the RSS-based solutions, various experiments demonstrate that multiple effects are of concern for the location precision. For
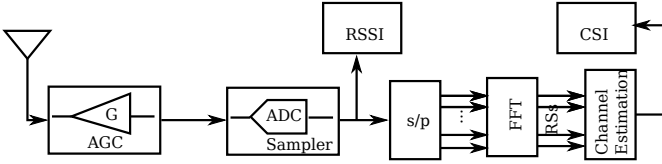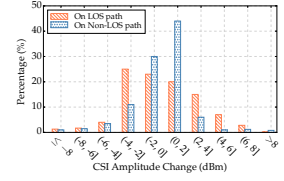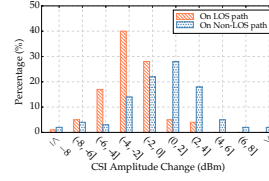
Figure 1: Flow diagram of signal processing in 802.11n standard

(a) Measurements at Subchannel 3 (b) Measurements at Subchannel 14

Figure 2: Amplitude change of CSI readings in different subchannels
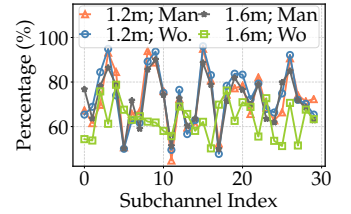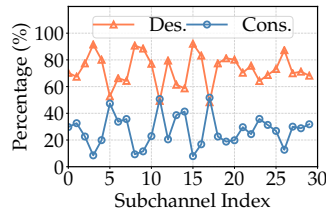

Figure 3: The probability from all the 30 subchannels that the CSI measurement changes result in constructive or destructive effect respectively when a subject blocks the LOS path in the area of interest

Figure 4: The probability from all the 30 subchannels that the CSI measurement changes result in constructive effect for subjects with various height when the radio devices are placed at a height of 1.2*m* and 1.6*m* respectively.

instance, in [49], Xu et. al have a subject stand within the Line-of-Sight (LOS) path between a single channel TX-RX link in a cluttered indoor environment and find that the blocking of the LOS path induced by humans may not lead to a decrease in RSS, which demonstrates the unpredictability of mulitipath fading induced bias. In the context of MIMO-OFDM, since the RSS is no longer a reliable indicator for the entire channel quality [16], in this section, we investigate the challenges posed by CSI measurements in solving the location estimate problem of cluttered environments. As aforementioned, both amplitude and phase information can be attained from CSI readings. Regarding the phase information, as also mentioned in [54], [47], [45], [29], compared with amplitude information, it contains significant random noise and, without phase correction and sanitization, cannot be leveraged for RF sensing applications. Therefore, we solely adopt the CSI amplitude measurements to design our indoor localization system.

To verify the multipath fading of subchannels, we carry out experiments in a typical domestic home and install a transmitter (access point) and a receiver (laptop) within a distance of 4 meters at a height of $1.4m$ from the floor. As we need to explore the signal fluctuation of CSI measurements before and after blocking the LOS path, at first, the CSI measurements are recorded when no subject is present in the room. Then, we gather CSI readings while a subject stands in or out of the LOS path and extract the average values of non-subject occupied CSI measurements from them. We coin the term of *destructive (or constructive) probability* to refer to the probability that the amplitude of the CSI measurement from a subchannel decreases (or increases) induced by the presence of a subject in the area of interest. Figure 3 illustrates the destructive and constructive probability of the CSI measurement changes from all 30 subchannels respectively when a subject blocks the LOS path. From this figure, we observe that the human-induced CSI change in LOS areas can be destructive as well as constructive. More specifically, for two certain subchannels, Figures 2a, and 2b show the histograms of the CSI amplitude change from subchannel 3 and 14 in both LOS and NLOS areas. From Figure 2a, we notice that the amplitude of CSI measurements in subchannel 3 decreases with probability of over 90% due to the blocking of the LOS path, while for subchannel 14, the strength of the signal attenuates with a probability smaller than 60%. From these figures, we conclude that the CSI measurements observed over diverse subchannels change in an unpredictable manner. Therefore, rather than employing a deterministic model of CSI measurements to estimate the distance, we propose to exploit a probabilistic approach for location discrimination.

Another underlying assumption of our system is that the height of the tracking subjects is higher than that of radio devices and resilient to different persons. To validate this, we select two different representative subjects (a man with height of $1.8m$ and a woman with height of $1.5m$) to conduct the identical experiments with the setup. Figure 4 quantifies the constructive probability of the CSI measurement changes from all 30 subchannels for different persons at various deployment height of AP and laptop, which validates our assumption. These results are due to fewer number of impacted signal paths once the height of an subject is lower than that of radio devices. Likewise, subjects with various height experience similar signal variation when the placement of radio devices is below the height of them.

IV. System Design

A. Problem Formulation

Here, we formulate the indoor localization problem and define the terms and variables used in our system. Let us consider a cluttered indoor environment, which is rich of multipath propagation. We virtually divide the space into a set of small square cells with the same size, say a set $\mathcal{K}$ of K cells. Within the area of interest, we deploy m transmitters (TX) and n receivers (RX), forming a set $\mathcal{L}$ of $L = n \cdot m$ TX-RX links. We denote L-dimensional CSI measurement space as $\mathbb{C}$. In $\mathbb{C}$, each value is L-dimensional vector, where every element is a *CSI reading vector* from a TX-RX link. As mentioned in Section III-A, we refer to this *CSI reading* vector as $\mathcal{C}$.

During the training phase, a CSI measurement fingerprint

map is built. To construct it, we have a subject stand at all $\mathcal{K}$ cells and, at each cell k, we collect a number of T CSI readings from all L links, forming the fingerprint map, $\mathcal{C}_{\text{map}}$. Concretely, let $\mathcal{C}_k^t(l)$ be the t-th CSI reading vector collected at cell k from the l-th link. Hence, The collected T CSI readings at cell k from the l-th link can be presented as $\mathcal{C}_k(l) = \{\mathcal{C}_k^1(l), \mathcal{C}_k^2(l), ..., \mathcal{C}_k^T(l)\}$. For the CSI readings from all L links at cell k, it can be presented as $\mathcal{C}_k = \{\mathcal{C}_k(1), ..., \mathcal{C}_k(l), ..., \mathcal{C}_k(L)\}$. Therefore, the stored CSI readings in the fingerprint map can be represented as $\{\mathcal{C}_1, \mathcal{C}_2, ..., \mathcal{C}_K\} = \mathcal{C}_{\text{map}}$.

During the online test operation, when a person is present in the monitored area, we gather a CSI reading vector without the cell number, say $\mathcal{C}_{\text{test}}$. Therefore, the location problem becomes, given a CSI measurement vector received in the online phase, $\mathcal{C}_{\text{test}} = \mathcal{C}$, we want to find a cell y which maximizes the probability $P(Y = y | \mathcal{C}_{\text{test}} = \mathcal{C})$ using the prior knowledge in the radio map, $\mathcal{C}_{\text{map}}$.

B. Probabilistic Method for Location Discrimination

As aforementioned, due to the random and unpredictable characteristics of CSI measurements, we propose a probabilistic fingerprint-based indoor localization system. More specific, we adopt Bayes estimator for the positioning problem. Since Bayes classifier is derived based on the Bayes' theorem, the conditional probability that a fingerprint $\mathcal{C}_{\text{test}} = \mathcal{C}$ collected during the test phase belongs to a certain cell $Y = y$ is given by

$$P(Y = y | \mathcal{C}_{\text{test}} = \mathcal{C}) = \frac{P(\mathcal{C}_{\text{test}} = \mathcal{C} | Y = y) \cdot P(Y = y)}{P(\mathcal{C}_{\text{test}} = \mathcal{C})}, \quad (1)$$

which is called posterior distribution. Obviously, the location discrimination problem of our system is to find the cell which maximizes the probability of posterior distribution, say $\hat{y} = \underset{y}{argmax}\, P(Y = y | \mathcal{C}_{\text{test}} = \mathcal{C})$.

Since we suppose that the targeted person resides within the area of interest without any biased place, we can safely consider that each location y is equally likely, and thus the probability of $P(Y = y)$ is the same at every cell[1]. Also, let $P(\mathcal{C}_{\text{test}} = \mathcal{C})$ be identical for all possible locations y, as we suppose we gather fingerprints across all the cells with the same possibility during the test phase. To find the optimal solution for the posterior distribution $P(Y = y | \mathcal{C}_{\text{test}} = \mathcal{C})$ is equivalent to having the maximum likelihood estimate of $P(\mathcal{C}_{\text{test}} | Y)$. More specifically, the predicted cell for the location of the subject is therefore $\hat{y} = \underset{y}{argmax}\, P(\mathcal{C}_{\text{test}} = \mathcal{C} | Y = y)$.

As addressed in existing researches (cf. [10]), we model the amplitude of every CSI reading at location y to approximately follow a *multivariate Gaussian distribution* with mean μ_y and common covariance matrix Σ. Therefore likelihood estimate of $P(\mathcal{C}_{\text{test}} | Y)$ is described mathematically as

$$P(\mathcal{C}_{\text{test}} = x | Y = y) = \frac{1}{\sqrt{(2\pi)^p |\Sigma|}} e^{-\frac{1}{2}(x - \mu_y)' \Sigma^{-1}(x - \mu_y)}, \quad (2)$$

where $p = L \cdot t \cdot r \cdot w$.

To estimate the parameters μ_y and Σ, we utilize the fingerprint map collected at training phase. The process is detailed as follows. At first, we convert Equation (2) to an equivalent description in the log-scale as

$$\delta(x|y) = -\frac{1}{2}\ln(|\Sigma|) - \frac{1}{2}(x - \mu_y)' \Sigma^{-1}(x - \mu_y) - \frac{y}{2}\ln(2\pi). \quad (3)$$

Given the set of T training CSI readings at cell y in the fingerprint map, $\mathcal{C}_y = \{\mathcal{C}_y^1, \mathcal{C}_y^2, ..., \mathcal{C}_y^T\}$, we assume each CSI measurement, $\mathcal{C}_y^t$, $t \in [1, T]$, to be i.i.d[2]. Then, taking the derivative w.r.t. μ_y of log-likelihood function (Equation (3)) and setting it to 0, we obtain

$$\hat{\mu}_y = \frac{1}{T}\sum_{t=1}^{T} \mathcal{C}_y^t.$$

Similarly, we take its derivative w.r.t. Σ^{-1} of (Equation (3)) and let it be 0, leading to

$$\hat{\Sigma} = \frac{1}{T}\sum_{t=1}^{T}(\mathcal{C}_y^t - \hat{\mu}_y)(\mathcal{C}_y^t - \hat{\mu}_y)'.$$

Therefore, using the collected fingerprint map, $\mathcal{C}_{\text{map}}$, the CSI readings at cell y, $\mathcal{C}_y$ can be represented by a multivariate Gaussian distribution with mean $\hat{\mu}_y$ and covariance matrix $\hat{\Sigma}$. In the test phase, using the collected CSI readings $\mathcal{C}_{\text{test}}$ and substituting the two parameters $\hat{\mu}_y$ and $\hat{\Sigma}$ into Equation (2), we can calculate the probability of generating these CSI readings at cell y. Once the system yields the probability of $\mathcal{C}_{\text{test}}$ at every cell, the cell in which we achieve the optimal probability, say $\hat{y}_{\text{op}}$, is exactly the estimated location of the subject.

C. Dimensionality Reduction

To apply indoor location systems into some practical large-scale scenarios, one main concern that pose a challenge in positioning a subject in real time is the high dimensionality of the data set. A large number of solutions have been proposed for the raised issue in RSS-based indoor localization systems (cf. [50], [11]). Since we leverage CSI measurements as the source signals, which has a much higher dimension than RSS indicators, so that it is severer to solve the problem that the high dimensional CSI readings bring about.

In this study, we adopt *principal component analysis (PCA)* to project every CSI reading in the data set to a lower dimensional subspace. In particular, assuming that we would like to reduce each *p-dimensional* CSI measurement to a *q-dimensional* vector ($q < p$), we require to choose the q dimensionalities with largest variances and ignore the other less significant ones. These resulting *q-dimensional* features are called *principal components*.

For our system, we take the following procedures to calculate the q principal components. At each location y, we have T p-dimensional vectors, $\mathcal{C}_y = \{\mathcal{C}_y^1, \mathcal{C}_y^2, ..., \mathcal{C}_y^T\}$. We write $\mathcal{C}_y'$ as a $T \times p$ data matrix $\mathcal{D}$. Since PCA requires a mean-centered matrix $\mathcal{U}$ in order to calculate variations, the first step for projecting CSI vectors is to find the mean vector γ of the data matrix $\mathcal{D}$ and subtract it from each row vector of $\mathcal{D}$ to obtain $\mathcal{U}$, where $\gamma = (\frac{1}{T}\sum_{t=1}^{T}\mathcal{C}_y^t)'$. Let $\mathcal{V}$ be the covariance matrix of $\mathcal{U}$, which can be computed

---

[1]If we have the prior knowledge about the user profile, the probability of $P(Y = y)$ is a constant variable and can be used in Equation (1).

[2]Our assumption is that every CSI reading has the same probability distribution and is independent with each other.

by $\mathcal{V} = \mathcal{U}'\mathcal{U}/T$. Then we can calculate p eigenvectors and eigenvalues of $\mathcal{V}$. We can form the $p - q$ PCA projection matrix by choosing the q eigenvectors of $\mathcal{V}$ which have the q largest eigenvalues $\Phi_{pca} = [x_{1,}^{pca} \, x_{2,}^{pca} \, ... \, x_q^{pca}]$. For any p-dimensional CSI vector $\mathbf{d} = (\boldsymbol{C}_y^i)' = (d_1, d_2, ... d_p)$, collected at location y, we project it into a corresponding q-dimensional vector by $\mathbf{d}_{pca} = (\mathbf{d} - \gamma) \cdot \Phi_{pca.}$

V. TRACKING

In this section, we investigate the implementation of two Bayesian estimators including Kalman filter (KF) and particle filter (PF) for continuously tracking the trajectory of a moving person. Firstly, we review the derivation of KF and PF and theoretically analyze the availability of the two Bayesian Estimators to their typical estimation problems. Then, we present the formulation of our tracking problem and derive the CRB from the proposed tracking model in the estimation context which can be solved using KF and PF.

A. Bayesian Estimators

Assuming the parameters needed to be estimated are packed in a *state vector*, $\mathbf{x}$, an estimation problem is to predict the state vector using given information including system model, control input and measurement model. Mathematically, the system model is written as

$$\mathbf{x}_k = f(\mathbf{x}_{k-1}, \mathbf{u}_{k-1}, \mathbf{w}_k) \quad (4)$$

and the measurement is modeled as

$$\mathbf{z}_k = h(\mathbf{x}_k, \mathbf{v}_k) \quad (5)$$

where $\mathbf{x}_k$ is the *state vector* at the k-th iteration, $f(\cdot)$ is the system dynamics function, $\mathbf{u}_k$ is system input, $\mathbf{w}_k$ is the process noise, $h(\cdot)$ is the measurement function and $\mathbf{v}_k$ is the measurement noise.

Upon the basic laws of probability, Bayesian filtering techniques solve the estimation problem by recursively predicting the probability density function (PDF) of current state vector $(\mathbf{x}_k)$ with the prediction stage and measurement update stage, which can be expressed as follows:

Prediction: predict the current state, $\mathbf{x}_k$, using previous measurements up to $(k-1)$-th iteration by

$$p(\mathbf{x}_k \,|\, \mathbf{z}_{1:k-1}, \mathbf{u}_{0:k-1}) = \begin{array}{c} \int p(\mathbf{x}_k \,|\, \mathbf{x}_{k-1}, \mathbf{u}_{1:k-1}) \\ \cdot p(\mathbf{x}_{k-1} \,|\, \mathbf{z}_{1:k-1}, \mathbf{u}_{0:k-2}) d\mathbf{x}_{k-1} \end{array} \quad (6)$$

Update: update the predicted $\mathbf{x}_k$ using the measurement obtained at k-th iteration by

$$p(\mathbf{x}_k \,|\, \mathbf{z}_{1:k}, \mathbf{u}_{0:k-1}) = \frac{g(\mathbf{z}_k \,|\, \mathbf{x}_k) \cdot p(\mathbf{x}_k \,|\, \mathbf{z}_{1:k-1}, \mathbf{u}_{0:k-1})}{p(\mathbf{z}_k \,|\, \mathbf{z}_{1:k-1}, \mathbf{u}_{0:k-1})}, \quad (7)$$

where $g(\mathbf{z}_k \,|\, \mathbf{x}_k)$ is the likelihood, $p(\mathbf{x}_k \,|\, \mathbf{z}_{1:k-1}, \mathbf{u}_{0:k-1})$ is prior probability and $p(\mathbf{x}_k \,|\, \mathbf{z}_{1:k}, \mathbf{u}_{0:k-1})$ is posterior probability.

1) Kalman Filtering

If the conditions that 1) both system model $f(\cdot)$ and measurement model $h(\cdot)$ are linear functions of state vector $\mathbf{x}_k$

and input $\mathbf{u}_k$, and 2) both system noise $\mathbf{w}_k$ and measurement noise $\mathbf{v}_k$ are Gaussian noise are satisfied, Equation (4) and (5) can be written in the form as

$$\mathbf{x}_k = \mathbf{A}\mathbf{x}_{k-1} + \mathbf{T}\mathbf{u}_{k-1} + \mathbf{w}_k, \quad (8)$$
$$\mathbf{z}_k = \mathbf{H}\mathbf{x}_k + \mathbf{v}_k, \quad (9)$$

where $\mathbf{A}$ is the *state transition matrix*, $\mathbf{T}$ is the *input matrix* and $\mathbf{H}$ is the *measurement matrix*. With these conditions, the prior and posterior PDF in Equation (6) and (7) can be analytically calculated by Kalman Filter algorithm as described in [41].

2) Particle Filtering

For nonlinear systems or non-Gaussian noise systems, it is impossible to analytically calculate the posterior PDF in Equation (7), since the calculation of the prior PDF ((6)) requires integration over the state space. For the objective of estimating these systems, PF is applied to approximate Equation (7) with a number of particles, which can be expressed as:

$$p(\mathbf{x}_k \,|\, \mathbf{z}_{1:k-1}, \mathbf{u}_{0:k-1}) \approx \sum_{m=1}^{M} w_k^m \delta(\mathbf{x}_k - \xi_k^m) \quad (10)$$

where ξ_k^m is the m-th particle at the k-th iteration, w_k^m is the normalized weight of ξ_k^m, $\delta(\cdot)$ is Dirac delta function and M is the number of particles. Therefore, to approximate the posterior PDF is equivalent to calculate the weight of each particle. With the adoption of sequential sampling importance resampling (SIR) PF [3], the weight of each particle can be calculated as

$$w_k^m \propto w_{k-1}^m \frac{g(\mathbf{z}_k \,|\, \xi_k^m) p(\xi_k^m \,|\, \xi_{k-1}^m)}{q(\xi_k^m \,|\, \xi_{k-1}^m, \mathbf{z}_k)}, \quad (11)$$

where $q(\cdot)$ is the importance density function.

As demonstrated in Algorithm 1, the SIR PF algorithm iteratively works in three procedures : 1) *sampling*, 2) *weight calculation* and 3) *resampling*.

B. Cramér-Rao Bound for Bayesian Filtering

The Cramér-Rao Bound (CRB) can provide a lower bound on the mean square error (MSE) of any unbiased estimator [37], [36]. As for Bayesian filtering, Let C_k denote the CRB of the estimated state vector $\mathbf{x}_k$, which is the inverse of the bayesian information (BIM) $J_k = C_k^{-1}$. Also, let Δ_φ^η be the partial derivatives with respect to vector η and φ. Following [36], the BIM can be calculated in a recursive way

$$J_{k+1} = \Omega_k - (D_k^{12})^T (D_k^{11} + J_k)^{-1} D_k^{12} + \Gamma_{k+1}, \quad (12)$$

where

$$D_k^{11} = E_\mathbf{x} \left\{ -\Delta_{\mathbf{x}_k}^{\mathbf{x}_k} \ln p(\mathbf{x}_{k+1} \,|\, \mathbf{x}_k) \right\} \quad (13)$$
$$D_k^{12} = E_\mathbf{x} \left\{ -\Delta_{\mathbf{x}_k}^{\mathbf{x}_{k+1}} \ln p(\mathbf{x}_{k+1} \,|\, \mathbf{x}_k) \right\} \quad (14)$$
$$\Omega_k = E_\mathbf{x} \left\{ -\Delta_{\mathbf{x}_{k+1}}^{\mathbf{x}_{k+1}} \ln p(\mathbf{x}_{k+1} \,|\, \mathbf{x}_k) \right\} \quad (15)$$
$$\Gamma_{k+1} = E_{\mathbf{z}, \mathbf{x}} \left\{ -\Delta_{\mathbf{x}_{k+1}}^{\mathbf{x}_{k+1}} \ln p(\mathbf{z}_{k+1} \,|\, \mathbf{x}_{k+1}) \right\} \quad (16)$$
$$J_0 = E_\mathbf{x} \left\{ -\Delta_{\mathbf{x}_0}^{\mathbf{x}_0} \ln p(\mathbf{x}_0) \right\}. \quad (17)$$

Algorithm 1 Sequential Importance Sampling with Resampling

• Draw a particle ξ_0^m from $\xi_0^m \sim p_0(\mathbf{x}_0)$ and set $w_0^m = 1/M$, $m = 1, ..., M$
▷In the first place, initialize M particles from the distribution $p_0(\mathbf{x}_0)$ and set their weight is equally likely.
• **For** $k = 1, ..., N$ recursively **do**
    1. Sampling
    – Draw $(\xi_k^m, \ m = 1, ..., M)$ from $\xi_k^m \sim p(\mathbf{x}_k \,|\, \xi_{k-1}^m)$
    2. Weight Calculation
    – Compute the updated importance weights

$$w_k^m = \frac{g(\mathbf{z}_k \,|\, \xi_k^m) p(\xi_k^m \,|\, \xi_{k-1}^m)}{q(\xi_k^m \,|\, \xi_{k-1}^m, \mathbf{z}_k)}$$

    3. Resampling
    – Normalize importance weights

$$w_k^m = \frac{w_k^m}{\sum_{n=1}^{M} w_k^n}, \ m = 1, ..., M$$

    – Resample particles according to importance weights

$$\{\xi_k^m, \ 1/M\} \leftarrow \{\xi_k^m, \ w_k^m\}, \ m = 1, ..., M$$

• **End for**

C. Tracking with Bayesian Estimators

1) Tracking System Model

In our tracking system, we assume the targeted person to walk with nearly constant velocity, hence, the motion of the subject within the time interval Δt from k to $k + 1$ can be described by an approximately fixed velocity with random acceleration. Let the state vector $\mathbf{x}_k$ be defined as $\mathbf{x}_k = [px_k, py_k, vx_k, vy_k]'$, where (px_k, py_k) and (vx_k, vy_k) is the coordinate and velocity of the subject respectively. The system model is

$$\mathbf{x}_{k+1} = A\mathbf{x}_k + Bn_k,$$

where

$$\mathbf{A} = \begin{bmatrix} 1 & 0 & \Delta t & 0 \\ 0 & 1 & 0 & \Delta t \\ 0 & 0 & 1 & 0 \\ 0 & 0 & 0 & 1 \end{bmatrix}, \mathbf{B} = \begin{bmatrix} \frac{1}{2}\Delta t^2 \\ \frac{1}{2}\Delta t^2 \\ \Delta t \\ \Delta t \end{bmatrix}.$$

We assume that the random acceleration n_k at any time interval Δt is a zero mean white Gaussian noise with the same variance, say $n_k \in \mathcal{N}(0, \sigma_n^2)$. Let the covariance of Bn_k be Q_k. Since both n_k and $\mathbf{B}$ do not depend on k, Q_k is expressed as $Q_k = \sigma_n^2 BB^T$.

For measurement model, since we can directly measure the coordinate $\mathbf{z}_k = (\widetilde{px_k}, \ \widetilde{py_k})$ of the tracked person from our localization system, the measurement equation of our tracking system is formulated as

$$\widetilde{px_k} = px_k$$
$$\widetilde{py_k} = py_k \tag{18}$$

hence, the measurement matrix $\mathbf{H}$ is given by

$$\mathbf{H} = \begin{bmatrix} 1 & 0 & 0 & 0 \\ 0 & 1 & 0 & 0 \end{bmatrix}.$$

We denote the noise of measurement $\mathbf{z}_k$ be $\mathbf{u}_k$, which follows zero-mean normal distribution $\mathbf{R}_k$. More specifically, let the two-dimensional vector $\mathbf{u}_k$ be defined as $\mathbf{u}_k = \begin{bmatrix} \mathbf{u}_k^x \\ \mathbf{u}_k^y \end{bmatrix}$, where $\mathbf{u}_k^x$, $\mathbf{u}_k^y$ are the measurement noise at x-axis and y-axis respectively. We assume they are uncorrelated and have identical variance, say $\mathbf{u}_k^x = \mathbf{u}_k^y \in \mathcal{N}(0, \sigma_u^2)$.

Therefore, under the circumstance of this tracking system, the equations (13)-(16) can be computed as

$$D_k^{11} = \mathbf{A}^T \mathbf{Q}_k^{-1} \mathbf{A} \tag{19}$$
$$D_k^{12} = -\mathbf{A}^T \mathbf{Q}_k^{-1} \tag{20}$$
$$\Omega_k = \mathbf{Q}_k^{-1} \tag{21}$$
$$\Gamma_{k+1} = \mathbf{H} \mathbf{R}_{k+1}^{-1} \mathbf{H}. \tag{22}$$

Applying the recursion form described in [2], the CRB on our tracking system can be expressed as

$$C_{k+1}^{-1} = J_{k+1} = (\mathbf{Q}_k + \mathbf{A} J_k^{-1} \mathbf{A}^T)^{-1} + \mathbf{H} \mathbf{R}_{k+1}^{-1} \mathbf{H}. \tag{23}$$

2) Tracking with KF and PF

Our tracking system can be modeled to satisfy the conditions of KF estimator. Concretely, assuming the subject walks with fixed velocity in the indoor environments, for this case, the assumption of $n_k \in \mathcal{N}(0, \sigma_n^2)$ holds.

In the realistic scenarios of our tracking system, we also allow the person to walk with random velocity and acceleration. Under this circumstance, the assumption of $n_k \in \mathcal{N}(0, \sigma_n^2)$ is not true, so that the conditions for KF cannot be satisfied. In this case, PF is applied for estimating the trajectory of the subject by approximating the posterior PDF using state particles.

For applying the Algorithm 1 into our tracking problem, we suppose $p_0(\mathbf{x}_0) = \mathcal{N}(\mathbf{x}_0; \ 0, \ \sigma)$ and $p(\mathbf{x}_k \,|\, \xi_{k-1}^m) = \mathcal{N}(\mathbf{x}_k; \ \xi_{k-1}^m + v_e(\xi_{k-1}^m) \cdot t_h, \ \sum_{k-1}^m)$, where $v_e(\xi_{k-1}^m)$ is the velocity of the m-th particle at the $(k-1)$-th iteration and $\sum_{k-1}^m$ is the covariance matrix of this distribution. We approximate the velocity as $v_e(\xi_{k-1}^m) = \xi_{k-1}^m - \xi_{k-2}^m$. Also, the importance density function $q(\mathbf{x}_k \,|\, \mathbf{x}_{k-1}^m, \mathbf{z}_k)$ we chose is equal to $p(\mathbf{x}_k \,|\, \mathbf{x}_{k-1}^m)$ and weight is set to $w_{k-1}^m = 1/M$. Therefore, the weight update equation can be given by $w_k^m \propto g(\mathbf{z}_k \,|\, \xi_k^m)$.

Since the likelihood, $g(\mathbf{z}_k \,|\, \mathbf{x}_k)$, is equivalent to the measurement function $\mathbf{y}_k = h(\mathbf{x}_k) + v_k$ and in our system, we model the measurement function as $\mathbf{z}_k = \mathbf{x}_k + \mathbf{u}_k$, where $\mathbf{u}_k \sim \mathcal{N}(0, \mathbf{R}_k)$, hence, $w_k^m = \mathcal{N}(y_k^m; \xi_k^m, \mathbf{R}_k)$.

VI. EXPERIMENTAL SETUP

A. Hardware Description and Data Aggregation

To evaluate the performance of our system, we deploy a wireless sensing network to aggregate required CSI measurements as our testbed. In our study, we use TP-LINK WR841N wireless APs with an IEEE 802.11n compliant radio operating in the 2.4GHz unlicensed band as transmitters. The receivers utilized in our system are *lenovo* laptops integrated with Intel WiFi Wireless Link 5300 Cards. By using the modified driver released by [16], the receivers can probe one CSI reading per packet. The placement of APs and laptops is fixed and known a priori. Each laptop deployed in the targeted environment is

synchronized with each other and receives 10 beacons from each AP per second.

During the training phase, we collect CSI measurements from a male volunteer with a height of $176cm$. Specifically, in all the experiment settings, to aggregate the training data and construct the fingerprint map, we divide the indoor areas of interest into $0.75m \times 0.75m$ cells and record 100 CSI readings (approximately 10 seconds) from every TX-RX link in each cell. Note that all laptops can receive packets from all APs concurrently, since we run multiple processes to download data from the IP addresses of corresponding APs. To mitigate the bias induced by different orientation and movement, we collect 5 datasets (500 CSI measurements) in which the subject faces towards four different directions and walks randomly within a specific cell. During the test phase, a different subject (a female participant with a height of $160cm$) is located at a random cell with random orientation. The subject may either stand still or walk at the cell. We collect CSI measurements at 500 locations (some locations are tested multiple times) and record samples with a duration of $5s$ (roughly 50 values) per cell.

B. Experiment Layouts

To confirm the validity of our system on various experimental scenarios, we carry out experiments in 4 different indoor environments. These environments are used for diverse functionalities and thus equipped with different domestic appliances and furnishings. As illustrated in Figure 5, Environment 1 is a corridor without any objects, Environment 2 and 3 are typical office environments with various space size and Environment 4 is domestic home equipped with household furniture. For all four indoor spaces, transmitters and receivers are placed as depicted in Figure 5.

C. Performance Metrics

We introduce three performance metrics to evaluate the performance of our proposed device-free indoor localization system.

1) Cell Estimation Accuracy

The cell estimation accuracy quantifies the ratio of the number of cells where the positions of the target person are correctly estimated during the test phase to that of all cell locations and is calculated as

$$\epsilon_{\text{test}} = \sum_{i=1}^{N_{\text{test}}} I(y_i = \hat{y}_i)/N_{\text{test}},$$

where N_{test} is the total number of testing cell locations.

2) Median Distance Error

At the test phase, we consider the location of a cell to be misclassified if the estimated cell does not match with the human occupied cell. Under such circumstances, we take into account the average mismeasured distance between the center points of the estimated cells and actual ones, termed as median distance error. Formally, the median distance error is given by

$$\sigma_{\text{test}} = \sum_{i=1}^{N_{\text{test}}} ||y_i - \hat{y}_i||/N_{\text{test}},$$

where $||y_i - \hat{y}_i||$ is the Euclidean distance between y_i and $\hat{y}_i$.

3) Average Processing Time

In our system, to address the problem of parameter estimation with high-dimensional datasets, we adopt PCA projection for dimension reduction. To validate the efficiency of PCA, the average processing time with different proportion of principle components to classify a testing location is measured on a MacBook Pro laptop (2.2 GHz Intel Core i7 processor, 16 GB 1600 MHz DDR3 memory, SSD storage).

VII. EXPERIMENTAL RESULTS

A. Comparing Various Localization Methods

In this section, we evaluate the performance of our system and compare it against other indoor localization systems including *Nuzzer* [31], *PC-DfP* [50] and *Pilot* [46]. The characteristics of these systems are summarized as follows:

- Nuzzer: *Nuzzer* is a RSS-based device-free indoor localization system which constructs an offline radio map at the training phase and then estimates the location of an entity using a *Bayesian-based inference* algorithm. In *Nuzzer*, the distribution of RSS follows the Gaussian assumption.
- PC-DfP: *PC-DfP* is also a Bayesian probabilistic classification based device-free indoor localization system using RSS measurements. To tailor the system to cluttered indoor environments, *PC-DfP* assumes that the density of the RSS mean vector of all the links at each location is *multivariate Gaussian* and adopts *linear discriminant analysis* for classification.
- Pilot: *Pilot* is a two-stage device-free indoor localization which exploits the *correlation feature* of CSI measurements to achieve a better performance compared to RSS-based schemes. *Pilot* will detect the presence of a human in the first stage and then trigger positioning phase to track the coordinate of the human in the second stage.

We conduct experiments in the 4 representative indoor environments as depicted in Section VI. Figure 6 and 7 illustrate the cell estimation accuracy and median distance error respectively. We should note that for *Pilot* it is possible that the system does not provide any prediction on the location. For this case, we define the error distance to be $min(width, length)$ of the testing room. In all indoor environments, we observe that our system outperforms the other three device-free localization systems. Compared to the RSS-based schemes (*Nuzzer*, *PC-DfP*), we attribute the better performance to more implicit information carried by CSI measurements in our system compared to RSS readings leveraged by *Nuzzer* and *PC-DfP*. Furthermore, in comparison with the other CSI-based localization system, *Pilot*, the performance gain of our system demonstrates that only one correlation feature and the two-stage location classification method adopted in *Pilot* are less effective than the location discrimination approach proposed in our system.

B. Impact of Principal Components

As aforementioned, parameter estimation is time-consuming due to the high-dimensionality of CSI vectors. In this section,
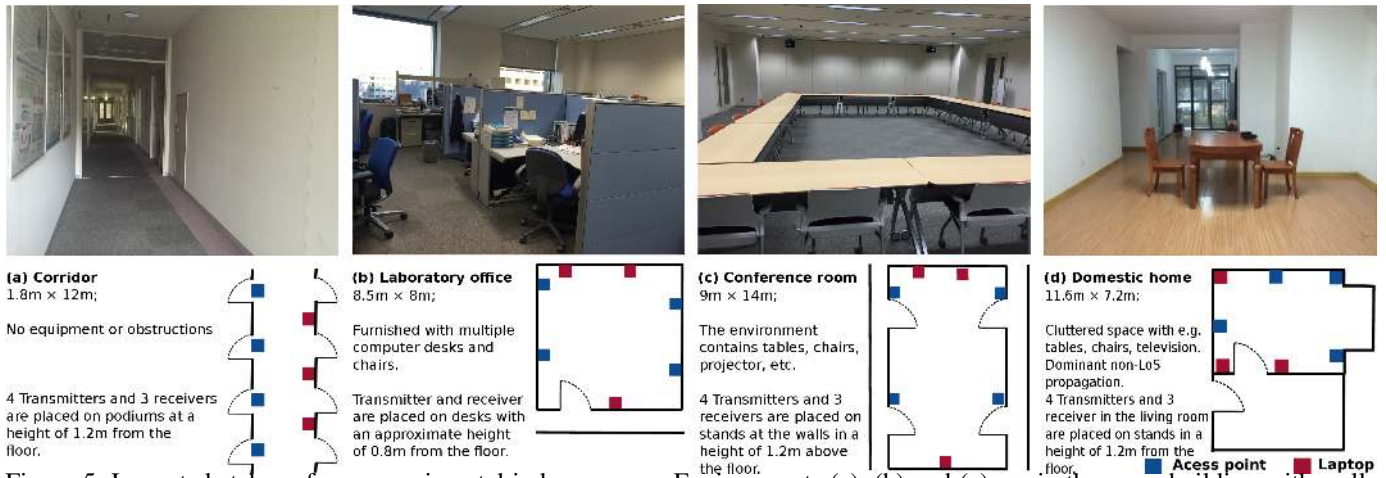
Figure 5: Layout sketches of our experimental indoor spaces. Environments (a), (b) and (c) are in the same building with walls mainly made of concrete. Environment (c) features a different penetration of walls which are made of wood and gypsum.
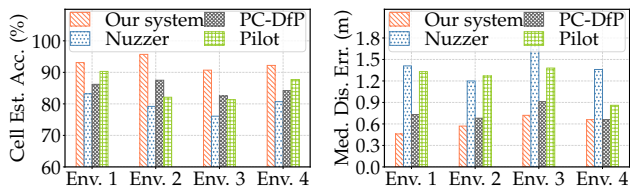

Figure 6: Comparison of cell estimation accuracy achieved by different indoor localization systems in four indoor environments
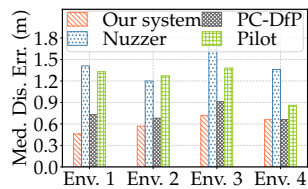
Figure 7: Comparison of median distance error achieved by different indoor localization systems in four indoor environments
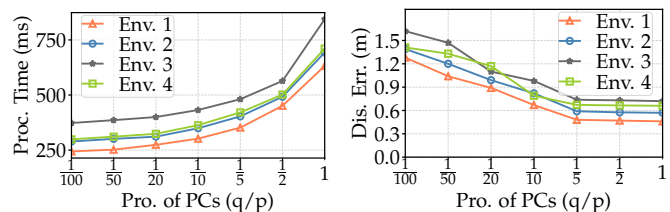
Figure 8: Average processing time to classify a test location with different proportion of principle components (PCs) in four indoor environments
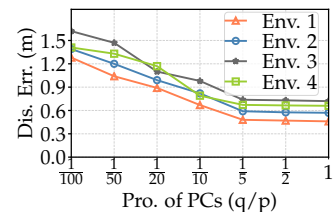
Figure 9: Median distance error with different proportion of principle components (PCs) in four indoor environments

we study the impact of using PCA dimensionality reduction on different evaluation metrics, including cell estimation accuracy (Figure 10), median distance error (Figure 9) and average processing time (Figure 8). From the three figures, we notice that a significant reduction in the PC-proportion (from 1 to 1/5) barely worsens the localization performance (see Figure 10 and 9), while dramatically saving processing time and thus improving the efficiency of our system (see Figure 8). Nonetheless, if we further reduce PCs (e.g. from 1/5 to 1/10), the classification accuracy will decline severely (see Figure 10) and error distance will hike sharply (see Figure 9); meanwhile the processing time can only reduce mildly, and its increasing rate progressively declines (see Figure 8). Thus, it is important to choose an appropriate number of PCs to balance the accuracy-efficiency trade-off for indoor localization.

C. Impact of Diverse Participants

To further validate that our system is resilient to diversity of participants, we recruited 8 subjects (6 males, 2 females; age: 23-31 years; height: 158-183 cm) to conduct the experiments in the environment of the domestic home and captured two datasets in two different days. We conduct three tests with different training data. First, we utilize the data of all 8 participants captured on one day for training and the 8 participants' CSI measurements from another day for testing. Then, we

evaluate the classification performance of our system for leave-one-out cross validation, in which the data from one subject captured on two different days is utilized for classification and the data from all the other subjects for training. Furthermore, for each subject, we measure localization accuracy using the data from one day for training and the data from another day as the classification data. Figure 11 shows the results, which demonstrate that three cases using distinct training data achieve comparable accuracy. Moreover, we also observe the use of the training data of all the 8 participants results in a slight increase in localization accuracy. In order to mitigate the impact of dataset diversity captured at different time, our system can perform a CSI calibration scheme, which further increases the performance of all the three cases. (see Section VII-F)

D. Influence of Data Aggregation Parameters

During the data aggregation procedure in our system, at each cell, we sample the CSI measurements from all the L TX-RX links, where each transmitter periodically broadcasts at a rate of P packets per second with a duration of T_{train} for the training phase and T_{test} for the test phase. Table I summarizes the default data aggregation parameters used in our experiments. In the following, we vary the values of these parameters and discuss
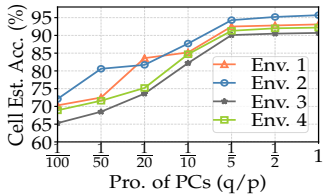
Figure 10: Cell estimation accuracy with different proportion of principle components (PCs) in four indoor environments
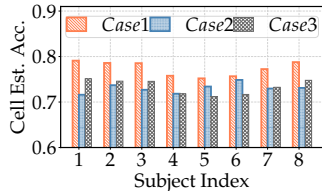
Figure 11: Impact of diverse participants for three cases using diverse training datasets

(a) Cell estimation accuracy of our localization scheme with different packet reception rate

(b) Average processing time to classify a test location with different packet reception rate

Figure 12: Influence of packet reception rate on the performance of our indoor localization system

(a) Cell estimation accuracy with different number of links

(b) Average processing time to classify a test location with different number of links

Figure 13: Influence of number of links on the performance of our indoor localization system

Table I: Default data aggregation parameters used in our experiments

Parameter	Notation	Default value
Number of links between TX-RX pairs	L	12
Packet broadcasting rate per second	P	10
Time duration for data aggregation per cell at training phase	T_{train}	$10s$
Time duration for data aggregation per cell at test phase	T_{test}	$5s$

the influence on the performance of our system.

1) Packet Reception Rate

From Figure 12a, we observe that we can achieve a cell estimation accuracy of over 90% by sampling the packets beyond a rate of 8 pks/s. This confirms a similar result reported in [35] for feasible RSS sample rates. Also, Figure 12b indicates that a reduced packet reception rate raises the performance of our system in terms of computation efficiency, which can be ascribed to the fewer data required to process a location.
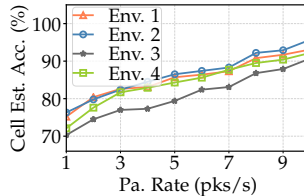
2) Number of Links

Aggregating data from fewer TX-RX links can lead to significant reduction on the computational complexity of our system. However, it may also lead to a decrease in terms of localization accuracy. The experimental results achieved with different number of links are shown in Figure 13a and 13b. The results support the above conclusion that a smaller number of links deteriorates the cell estimation accuracy and reduces the localization processing time.
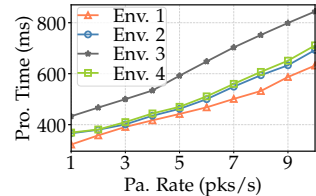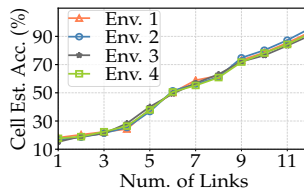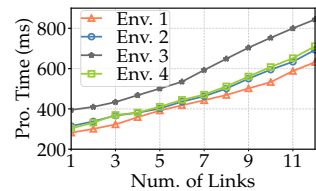
3) Time of Collecting Data

For fingerprint-based indoor localization schemes, the construction of a radio map is arduous, hence, reducing the time of collecting data at each cell can alleviate the effort during the training phase. With respect to the test phase, spending less time to collect the test measurements can make localization systems more responsive for locating the targeted people.

Table II (Table III) shows the average localization delay and the cell estimation accuracy/distance error with different time of collecting data during the training phase (test phase) using the same test dataset (training dataset) in all the indoor environments. There is a clear tradeoff between the cell estimation accuracy/distance error and localization delay with respect to the time of collecting data.

E. Tracking Results

1) Data Set

In the set of experiments, we collected datasets of CSI measurements when the targeted person is moving in all four indoor environments as depicted in Figure 5. More specifically, at each environment, the subject walks along a random trajectory in the spaces following two walking types: (1) fixed velocity (approximately $2m/s$) and (2) free-style velocity, at which the subject can walk at any speed or stand at a certain location, for about 5 minutes. To obtain the ground-truth information where the subject is walking, we record videos. Table IV lists the experimental parameters used in the

Table II: Influence of time frame of data aggregation on the performance of our indoor localization system during training phase

T_{train} (s)	2	4	6	8	10
Cell estimation accuracy (%)	84.4	88.5	88.9	91.7	92.9
Distance error (m)	0.77	0.72	0.73	0.68	0.60
Processing time (ms)	443	491	507	656	720

Table III: Influence of time frame of data aggregation on the performance of our indoor localization system during test phase

T_{test} (s)	1	2	3	4	5
Cell estimation accuracy (%)	79.5	82.1	89.8	91.7	92.9
Distance error (m)	0.86	0.80	0.74	0.66	0.60
Processing time (ms)	473	534	590	655	720

Table IV: Experimental parameters used in our tracking system

Parameter	Notation	Value
covariance of process noise for Kalman filter	$\mathbf{Q}_k$	$2I_4$
covariance of measurement noise for Kalman filter	$\mathbf{R}_k$	$5I_2$
number of particles for particle filter	M	1000
time frame of each iteration for both filters	t_h	$1s$

Figure 14: Estimated trajectories from both Kalman filter and particle filter when the subjects walk with random velocity at Env. 3.

Figure 15: CRB for tracking location compared to the performance of Kalman filter and particle filter when the subject walks with fixed velocity

Figure 16: CRB for tracking location compared to the performance of Kalman filter and particle filter when the subject walks with random velocity

Figure 17: Impact of diverse participants for three cases using diverse training datasets

study.

2) Tracking Accuracy

We use both filters described above to track the trajectories of the subject with two different walking styles. Note that participants are not restricted in their body motion during walking. Table V shows the mean absolute errors (MAEs) of various methods for each environment. As illustrated in this table, among all situations, applying the Kalman filter to the dataset of the subject moving with fixed velocity, achieves the best tracking precision with an average MAE of $0.63m$. This is a $0.17m$ improvement compared to particle filter based tracking with the same dataset. Whereas, when the subject mimics the walking style in real life (walk at random speed and stop freely), the average MAE at all the four indoor environments using particle filter is $0.92m$, a $0.31m$ improvement compared to that using Kalman filter. These results validate that Kalman filter is an optimal solution for linear dynamics systems (constant walking speed), in which all noise satisfies the normal distribution (we assume $\mathbf{Q}_k$ and $\mathbf{R}_k$ are Gaussian noise). Under nonlinear circumstances (free walking), the experimental results support the conclusion that particle filter is to be preferable to Kalman filter. More intuitively, for walking with random velocity at Env. 3, Figure 14 shows the tracking trajectory results from both Kalman filter and particle filter, from which we also observe that Kalman filter is inferior to particle filter for tracking the subjects with random walking velocity[3].

3) Comparison to the CRB

We further compare the tracking performance of KF and PF in the two scenarios against CRB on our modeling system recursively derived via Equation (23). The results achieved at the conference room are shown in Figures 15, 16 (Results achieved in the other three indoor environments are omitted due to space constraints. However, similar performance can be obtained compared to that at the conference room). As shown in Figure 15, with constant walking velocity, MSE computed by KF can achieve (or close to) the bound, which confirms that KF is an optimal filter under the conditions described in Section V-A1. In contrast, as plotted in Figure 16, when the motion of the subject is not nearly constant, the MSE of state estimates obtained from KF cannot achieve the bound because the random acceleration n_k is not a zero mean white Gaussian noise any further. Compared with the performance achieved by KF, MSE of state estimate derived from PF is

---

[3]Other figures of tracking trajectory results with different walking style performed at the other indoor spaces are omitted due to space constraints.
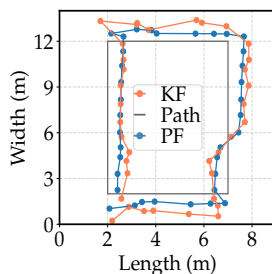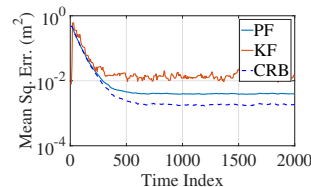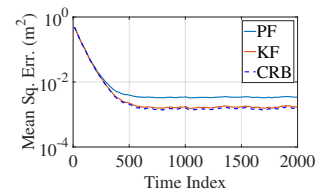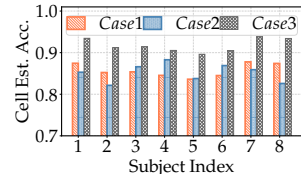

Table V: Average MAEs (in meters) from our proposed tracking approaches

	Env.1	Env.2	Env.3	Env.4
Kalman filter (fixed velocity)	0.57	0.66	0.77	0.63
Kalman filter (free-style velocity)	0.91	0.97	1.13	1.02
particle filter (fixed velocity)	0.63	0.70	0.81	0.69
particle filter (free-style velocity)	0.86	0.88	0.94	0.91

much closer to the bound since the averaged estimation error of weighted state measurement particles ξ_k^m, $m = 1, ..., M$, is much smaller than that achieved via Kalman filter equations.

F. Combating with Environment Dynamics

Our system relies on static indoor environments for constructing the radio map, however, over time, changes in the environment occur, such as temperature, humidity and placement of furnishings. As a consequence, the created training fingerprint map cannot precisely reflect the operational environment at a different time. Thus, the calibration of this training map will be required to alleviate the effect of environment changes. In the context of device-bound localization systems, some approaches in [15] have proposed to continuously calibrate the these systems and tailor them to time-varying phenomena. Inspired by [15], we propose a CSI adjustment scheme for system calibration. The rational for this scheme is that we assume, at any cell, the CSI change induced by the presence of a subject is irrelevant with time. Specifically, at time t_1, let CSI measurements of empty environment and cell k be $CSI_{t_1}^{em}$ and

Table VI: Localization results of two time-varying CSI measurement datasets with or without CSI calibration

	Case 1	Case 2	Case 3
	Acc. (%)	Acc. (%)	Acc. (%)
w/o calibration	77.6	72.2	70.4
w/ calibration	84.9	83.2	91.3

Table VII: Results of the different furniture layouts with or without CSI calibration

	Cell Estimation Accuracy (%)	Median Distance Error (m)
w/o calibration	64.8	1.58
w/ calibration	81.3	0.96

$CSI_{t_1}^k$ respectively. Likewise, at time t_2, $CSI_{t_2}^{em}$ and $CSI_{t_2}^k$ represent the CSI measurements of the two conditions. According to our assumption, we can obtain that $CSI_{t_1}^k$-$CSI_{t_1}^{em}$ = $CSI_{t_2}^k$-$CSI_{t_2}^{em}$. Hence, to adjust the CSI measurements at each cell at time t_2, we only need the information of CSI measurements of every cell at time t_1 and the change of CSI measurements induced by environment dynamics within the time interval from t_1 to t_2, say $CSI_{t_2}^{em}$-$CSI_{t_1}^{em}$. Based on this idea, when the subject is absent from the indoor environments, we routinely collect the CSI measurements and compute the variance of CSI measurements between two sequential periods, say ΔCSI^{em}, which can be used to correct every training CSI measurement in the fingerprint map. After each calibration, the training CSI measurement at cell k is updated via $CSI_{tr}^k + \Delta CSI^{em} \mapsto CSI_{tr}^k$. Note that the timings when to collect the CSI feature vector of empty environment are predefined, which should be determined accordingly. For instance, for domestic home, it can be measured when the subject is at work. As for the conference room, it can be collected out of office hours.

To validate the effectiveness of the CSI adjustment scheme, we sanitize the CSI measurements utilized in Section VII-C, two datasets of which are captured in two diverse days. After the CSI measurement configuration scheme, we re-evaluate the performance of the three cases mentioned in Section VII-C, results of which are shown in Figure 17. By comparing the results achieved with or without the CSI measurement adjustment in Figures 11 and 17, the localization performance of all the three cases is enhanced, each of which has an overall accuracy gain of 7.7%, 11.0% and 20.9% respectively, shown in Table VI.

We further conduct experiments in the conference room with a different furniture layout to validate the efficiency of the proposed calibration scheme (we remove some desks in this case). As Table VII shows, with the correction of CSI measurements, we can achieve an estimation accuracy of over 80%, an increase of 16% compared to that obtained without the CSI sanitization. Similarly, the performance of median distance error is also improved with the adjusted CSI measurements.

VIII. DISCUSSION

In this section, we discuss several unsolved issues in this paper and raise possible solutions to address these problems, which could further enhance the performance of our system.

A. Identification and Localization of Multiple Persons

One limitation of fingerprint-based techniques is that the training phase consumes a significant amount of time and effort. This situation is particularly true when we scale our system to simultaneously identifying multiple subjects, since the training overhead increases exponentially with all possible combinations of subjects. In the context of the device-based active localization systems, RF-propagation tool [30] and the approach in [23] are applied to ease the effort of the radio map construction. These techniques may be also experimented with our device-free system to generate different radio maps for multiple persons. Another promising solution might be to isolate multiple persons in separate spaces from each other and match them one by one using the known single-person radio map.

B. Using Different Hardware

IWL5300 is the first commodity wireless NIC which reports CSI information. Recently, other CSI tools, such as *Splicer* [47] and *Chronos* [38], enable to be integrated with other types of NIC cards by the modification of wireless drivers. Thus, another extension of our system is to consider the effect of using NIC cards from different vendors. The challenge for this case is the CSI samples captured in the training phase with one particular model of NIC vary considerably with those collected by another model of NIC in the test phase. One promising approach is that using a small number of recent CSI observations at some specific cells as new training samples to calculate the calibration parameters that then can used to update the radio map.

IX. CONCLUSION

We have presented a fingerprint-based device-free system that enables precise localization in indoor spaces. In our system, we aggregate the CSI measurements from commodity 802.11n WiFi devices, so that fine-grained subchannel information can be utilized to localize a subject. Classification is done comparing testing CSI readings with the CSI fingerprints and determine the location with highest probability by Bayes Classification. The performance of our system can be further enhanced by reducing dimensionality with PCA. The experimental evaluation in four different indoor environments shows that the system can outperform the state-of-the-art systems including *Nuzzer*, *PC-DfP* and *Pilot* in terms of both cell estimation accuracy and error distance. We further present a model for tracking the coordinates of the moving subject. Based on the tracking model, we derive the Cramér-Rao Bound which provides a lower bound for the mean square error of any estimators. We apply Kalman filter and Bayesian filter as two estimators for recursively predicting the coordinates of the moving target. Experimental results demonstrate that Kalman filter is a preferred option for tracking the subject with fixed walking speed, while particle filter is more robust to these scenarios where the subject walks randomly. Experimental results also show that the performance of Kalman filter can achieve the CRB, which further verify that it is an optimal estimator for the linear systems with additive white Gaussian noise.

REFERENCES

[1] Source: Strategy Analytics: http://www.strategyanalytics.com.

[2] B. Arulampalam. *Beyond the Kalman Filter: Particle Filters for Tracking Applications*. Artech House.

[3] M. Arulampalam, S. Maskell, N. Gordon, and T. Clapp. A tutorial on particle filters for online nonlinear/non-gaussian bayesian tracking. *Signal Processing, IEEE Transactions on*, 50(2):174–188, Feb 2002.

[4] P. Bahl and V. Padmanabhan. Radar: an in-building rf-based user location and tracking system. In *INFOCOM 2000. Nineteenth Annual Joint Conference of the IEEE Computer and Communications Societies. Proceedings. IEEE*, volume 2, pages 775–784 vol.2, 2000.

[5] M. Bocca, O. Kaltiokallio, N. Patwari, and S. Venkatasubramanian. Multiple target tracking with rf sensor networks. *Mobile Computing, IEEE Transactions on*, 13(8):1787–1800, Aug 2014.

[6] S. Cai, W. Liao, C. Luo, M. Li, X. Huang, and P. Li. Cril: An efficient online adaptive indoor localization system. *IEEE Transactions on Vehicular Technology*, 66(5):4148–4160, May 2017.

[7] X. Chen, A. Edelstein, Y. Li, M. Coates, M. Rabbat, and A. Men. Sequential monte carlo for simultaneous passive device-free tracking and sensor localization using received signal strength measurements. In *Information Processing in Sensor Networks (IPSN), 2011 10th International Conference on*, pages 342–353, April 2011.

[8] Y. Chen, D. Lymberopoulos, J. Liu, and B. Priyantha. Fm-based indoor localization. In *Proceedings of the 10th International Conference on Mobile Systems, Applications, and Services*, MobiSys '12, pages 169–182, New York, NY, USA, 2012. ACM.

[9] Z. Chen. Bayesian Filtering: From Kalman Filters to Particle Filters, and Beyond. Technical report, McMaster University, 2003.

[10] A. J. Coulson, A. G. Williamson, and R. G. Vaughan. A statistical basis for lognormal shadowing effects in multipath fading channels. *IEEE Trans. on Communications*, 46(4):494–502, 1998.

[11] G. Deak, K. Curran, and J. Condell. A survey of active and passive indoor localisation systems. *Computer Communications*, 35(16):1939 – 1954, 2012.

[12] A. Doucet, N. de Freitas, and N. Gordon. Sequential monte carlo methods in practice. In A. Doucet, N. de Freitas, and N. Gordon, editors, *Sequential Monte Carlo Methods in Practice*, Statistics for Engineering and Information Science. Springer New York, 2001.

[13] S. Feldmann, K. Kyamakya, A. Zapater, and Z. Lue. An indoor bluetooth-based positioning system: Concept, implementation and experimental evaluation. pages 109–113, 2003.

[14] B. Ferris, D. Fox, and N. Lawrence. Wifi-slam using gaussian process latent variable models. In *Proceedings of the 20th International Joint Conference on Artifical Intelligence*, IJCAI'07, pages 2480–2485, San Francisco, CA, USA, 2007. Morgan Kaufmann Publishers Inc.

[15] A. Haeberlen, E. Flannery, A. M. Ladd, A. Rudys, D. S. Wallach, and L. E. Kavraki. Practical robust localization over large-scale 802.11 wireless networks. In *Proceedings of the 10th Annual International Conference on Mobile Computing and Networking*, MobiCom '04, pages 70–84, New York, NY, USA, 2004. ACM.

[16] D. Halperin, W. Hu, A. Sheth, and D. Wetherall. Tool release: Gathering 802.11n traces with channel state information. *ACM SIGCOMM CCR*, 41(1):53, Jan. 2011.

[17] M. Hardegger, G. Tröster, and D. Roggen. Improved actionslam for long-term indoor tracking with wearable motion sensors. In *Proceedings of the 2013 International Symposium on Wearable Computers*, ISWC '13, pages 1–8, New York, NY, USA, 2013. ACM.

[18] M. Hazas and A. Hopper. Broadband ultrasonic location systems for improved indoor positioning. *Mobile Computing, IEEE Transactions on*, 5(5):536–547, May 2006.

[19] P. Hillyard, D. Maas, S. N. Premnath, N. Patwari, and S. K. Kasera. Through-wall person localization using transceivers in motion. *CoRR*, abs/1511.06703, 2015.

[20] M. Hossain, M. Hassan, M. Qurishi, and A. Alghamdi. Resource allocation for service composition in cloud-based video surveillance platform. In *Multimedia and Expo Workshops (ICMEW), 2012 IEEE International Conference on*, pages 408–412, July 2012.

[21] O. Kaltiokallio, H. Yigitler, and R. Jantti. A three-state received signal strength model for device-free localization. *IEEE Transactions on Vehicular Technology*, PP(99):1–1, 2017.

[22] K. Kunze, G. Bahle, P. Lukowicz, and K. Partridge. Can magnetic field sensors replace gyroscopes in wearable sensing applications? In *Wearable Computers (ISWC), 2010 International Symposium on*, pages 1–4, Oct 2010.

[23] H. Lim, L. C. Kung, J. C. Hou, and H. Luo. Zero-configuration, robust indoor localization: Theory and experimentation. In *Proceedings IEEE INFOCOM 2006. 25TH IEEE International Conference on Computer Communications*, pages 1–12, April 2006.

[24] L. M. Ni, Y. Liu, Y. C. Lau, and A. P. Patil. Landmarc: Indoor location sensing using active rfid. *Wirel. Netw.*, 10(6):701–710, Nov. 2004.

[25] K. Ohara, T. Maekawa, Y. Kishino, Y. Shirai, and F. Naya. Transferring positioning model for device-free passive indoor localization. In *Proceedings of the 2015 ACM International Joint Conference on Pervasive and Ubiquitous Computing*, UbiComp '15, pages 885–896, New York, NY, USA, 2015. ACM.

[26] V. Otsason, A. Varshavsky, A. LaMarca, and E. de Lara. Accurate gsm indoor localization. In *UbiComp 2005: Ubiquitous Computing*, volume 3660 of *Lecture Notes in Computer Science*, pages 141–158. Springer Berlin Heidelberg, 2005.

[27] G. Pirkl, K. Stockinger, K. Kunze, and P. Lukowicz. Adapting magnetic resonant coupling based relative positioning technology for wearable activitiy recogniton. In *Wearable Computers, 2008. ISWC 2008. 12th IEEE International Symposium on*, pages 47–54, Sept 2008.

[28] K. Qian, C. Wu, Z. Yang, Y. Liu, and K. Jamieson. Widar: Decimeter-level passive tracking via velocity monitoring with commodity wi-fi. In *Proceedings of the 18th ACM International Symposium on Mobile Ad Hoc Networking and Computing*, page 6. ACM, 2017.

[29] K. Qian, C. Wu, Z. Yang, Y. Liu, and Z. Zhou. Pads: Passive detection of moving targets with dynamic speed using phy layer information. In *2014 20th IEEE International Conference on Parallel and Distributed Systems (ICPADS)*, pages 1–8, Dec 2014.

[30] M. Scholz, L. Kohout, M. Horne, M. Budde, M. Beigl, and M. A. Youssef. Device-free radio-based low overhead identification of subject classes. In *Proceedings of the 2Nd Workshop on Workshop on Physical Analytics*, WPA '15, pages 1–6, New York, NY, USA, 2015. ACM.

[31] M. Seifeldin, A. Saeed, A. E. Kosba, A. El-keyi, and M. Youssef. Nuzzer: A large-scale device-free passive localization system for wireless environments. *IEEE Transactions on Mobile Computing*, 12(7):1321–1334, July 2013.

[32] S. Sen, B. Radunovic, R. R. Choudhury, and T. Minka. Precise indoor localization using phy layer information. In *ACM Hotnets*. ACM HotNets, November 2011.

[33] S. Sen, B. Radunovic, R. R. Choudhury, and T. Minka. You are facing the mona lisa: Spot localization using phy layer information. In *Proceedings of the 10th International Conference on Mobile Systems, Applications, and Services*, MobiSys '12, pages 183–196, New York, NY, USA, 2012. ACM.

[34] S. Shi, S. Sigg, and Y. Ji. Probabilistic fingerprinting based passive device-free localization from channel state information. In *Proceedings of the 2016 IEEE 83rd Vehicular Technology Conference: VTC2016-Spring*, VTC '16, 2016.

[35] S. Sigg, U. Blanke, and G. Troester. The telepathic phone: Frictionless activity recognition from wifi-rssi. In *IEEE International Conference on Pervasive Computing and Communications (PerCom)*, PerCom '14, 2014.

[36] P. Tichavsky, C. H. Muravchik, and A. Nehorai. Posterior cramer-rao bounds for discrete-time nonlinear filtering. *IEEE Transactions on Signal Processing*, 46(5):1386–1396, May 1998.

[37] H. Van Trees. *Detection, Estimation, and Modulation Theory*. Number pt. 1. Wiley, 2004.

[38] D. Vasisht, S. Kumar, and D. Katabi. Decimeter-level localization with a single wifi access point. In *13th USENIX Symposium on Networked Systems Design and Implementation (NSDI 16)*, pages 165–178, Santa Clara, CA, Mar. 2016. USENIX Association.

[39] J. Wang, X. Zhang, Q. Gao, H. Yue, and H. Wang. Device-free wireless localization and activity recognition: A deep learning approach. *IEEE Transactions on Vehicular Technology*, 66(7):6258–6267, July 2017.

[40] R. Want, A. Hopper, V. Falcão, and J. Gibbons. The active badge location system. *ACM Trans. Inf. Syst.*, 10(1):91–102, Jan. 1992.

[41] G. Welch and G. Bishop. An introduction to the kalman filter. Technical report, Chapel Hill, NC, USA, 1995.

[42] J. Wilson and N. Patwari. Through-wall tracking using variance-based radio tomography networks. *CoRR*, abs/0909.5417, 2009.

[43] J. Wilson and N. Patwari. Radio tomographic imaging with wireless networks. *Mobile Computing, IEEE Transactions on*, 9(5):621–632, May 2010.

[44] C. Wu, Z. Yang, Z. Zhou, Y. Liu, and M. Liu. Mitigating large errors in wifi-based indoor localization for smartphones. *IEEE Transactions on Vehicular Technology*, 66(7):6246–6257, July 2017.

[45] C. Wu, Z. Yang, Z. Zhou, K. Qian, Y. Liu, and M. Liu. Phaseu: Real-time los identification with wifi. In *2015 IEEE Conference on Computer Communications (INFOCOM)*, pages 2038–2046, April 2015.

[46] J. Xiao, K. Wu, Y. Yi, L. Wang, and L. Ni. Pilot: Passive device-free indoor localization using channel state information. In *Distributed Computing Systems (ICDCS), 2013 IEEE 33rd International Conference on*, pages 236–245, July 2013.

[47] Y. Xie, Z. Li, and M. Li. Precise power delay profiling with commodity wifi. In *Proceedings of the 21st Annual International Conference on Mobile Computing and Networking*, MobiCom '15, pages 53–64, New York, NY, USA, 2015. ACM.

[48] Y. Xie, J. Xiong, M. Li, and K. Jamieson. xd-track: leveraging multi-dimensional information for passive wi-fi tracking. In *Proceedings of the 3rd Workshop on Hot Topics in Wireless*, pages 39–43. ACM, 2016.

[49] C. Xu, B. Firner, R. S. Moore, Y. Zhang, W. Trappe, R. Howard, F. Zhang, and N. An. Scpl: Indoor device-free multi-subject counting and localization using radio signal strength. In *Proceedings of the 12th International Conference on Information Processing in Sensor Networks*, IPSN '13, pages 79–90, New York, NY, USA, 2013. ACM.

[50] C. Xu, B. Firner, Y. Zhang, R. Howard, J. Li, and X. Lin. Improving rf-based device-free passive localization in cluttered indoor environments through probabilistic classification methods. In *Proceedings of the 11th International Conference on Information Processing in Sensor Networks*, IPSN '12, pages 209–220, New York, NY, USA, 2012. ACM.

[51] M. Youssef, M. Mah, and A. Agrawala. Challenges: Device-free passive localization for wireless environments. In *Proceedings of the 13th Annual ACM International Conference on Mobile Computing and Networking*, MobiCom '07, pages 222–229, New York, NY, USA, 2007. ACM.

[52] D. Zhang, J. Ma, Q. Chen, and L. Ni. An rf-based system for tracking transceiver-free objects. In *Pervasive Computing and Communications, 2007. PerCom '07. Fifth Annual IEEE International Conference on*, pages 135–144, March 2007.

[53] Y. Zhao and N. Patwari. Noise reduction for variance-based device-free localization and tracking. In *Sensor, Mesh and Ad Hoc Communications and Networks (SECON), 2011 8th Annual IEEE Communications Society Conference on*, pages 179–187, June 2011.

[54] Z. Zhou, Z. Yang, C. Wu, W. Sun, and Y. Liu. Lifi: Line-of-sight identification with wifi. In *IEEE INFOCOM 2014 - IEEE Conference on Computer Communications*, pages 2688–2696, April 2014.

Stephan Sigg is an assistant professor at Aalto University in the Department of Communications and Networking. From October 2013 to September 2015, he was with the Computer Networks Group of Georg-August-University Goettingen. Before, he was a researcher at TU-Braunschweig and an academic guest in the Wearable Computing Lab at ETH Zurich and in the Nodes laboratory at University of Helsinki. From December 2010 to March 2013, Stephan was with the National Institute of Informatics (NII), in the Information systems architecture research division. He was a visiting Professor for Distributed and Ubiquitous Systems at the TU Braunschweig in the winter term 2010 and a PostDoc researcher at the chair for Pervasive Computing Systems (TecO) of the Karlsruhe Institute of Technology (KIT) in 2010 and a PostDoc researcher at the chair for Distributed and Ubiquitous Systems at the TU Braunschweig from 2008 to 2010. He obtained his PhD (Dr. rer. nat.; 2008) from University of Kassel where he was with the chair for Communication Technology (ComTec) from 2005 to 2007. His research interests include the design, analysis and optimisation of algorithms for distributed and ubiquitous systems.

Lin Chen is currently a Ph.D. student in the Department of Electrical Engineering, Graduate School of Arts and Sciences, Yale University. He received his B.S. degree in computer science from Peking University in 2014. His research interests focus on wireless networks and network theory.

Shuyu Shi is currently a research fellow in Wireless And Networked Distributed Sensing (WANDS) system group in Parallel and Distributed Computing Centre (PDCC), School of Computer Science and Engineering, Nanyang Technological University (NTU), Singapore. She obtained her PhD from SOKENDAI, where she was with National Institute of Informatics and Department of Informatics, Japan. She was also a JSPS Research Fellow from April 2015 to October 2016. She received her B.E. from University of Science and Technology of China(USTC) in 2011. Her research interests focus on mobile and ubiquitous computing.

Yusheng Ji received B.E., M.E., and D.E. degrees in electrical engineering from the University of Tokyo. She joined the National Center for Science Information Systems, Japan (NACSIS) in 1990. Currently, she is a Professor at the National Institute of Informatics, Japan (NII), and the Graduate University for Advanced Studies (SOKENDAI). Her research interests include network architecture, resource management, and quality of service provisioning in wired and wireless communication networks. She has served as a Board Member of Trustees of IEICE, Steering Committee Member of Quality Aware Internet (QAI) SIG and Internet and Operation Technologies (IOT) SIG of IPSJ, Associate Editor of IEICE Transactions and IPSJ Journal, Guest Editor-in-Chief, Guest Editor, and Guest Associate Editor of Special Sections of IEICE Transactions, Guest Associate Editor of Special Issues of IPSJ Journal, etc. She has also served as a TPC member of many conferences, including IEEE INFOCOM, ICC, GLOBECOM, VTC etc., and Symposium Co-chair of IEEE GLOBECOM 2012, 2014. She is an Editor of IEEE Transactions of Vehicular Technology, Track Co-chair of IEEE VTC 2016 Fall, and an Expert Member of IEICE Technical Committees on Internet Architecture, and Communication Quality.